Effect of confinement on anharmonic phonon scattering and thermal conductivity in pristine silicon nanowires

Zahid Rashid,[1,2] Liyan Zhu,[3] and Wu Li[1,*]

[1]*Institute for Advanced Study, Shenzhen University, Nanhai Avenue 3688, Shenzhen 518060, People's Republic of China*

[2]*Key Laboratory of Optoelectronic Devices and Systems of the Ministry of Education of Guangdong Province, College of Optoelectronics Engineering, Shenzhen University, 518060 Shenzhen, People's Republic of China*

[3]*School of Physics and Electronic and Electrical Engineering and Jiangsu Key Construction Laboratory of Modern Measurement Technology and Intelligent Systems, Huaiyin Normal University, Huai'an, Jiangsu, 223300, China*

(Received 21 December 2017; revised manuscript received 12 February 2018; published 28 February 2018)

The effect of confinement on the anharmonic phonon scattering rates and the consequences thereof on the thermal transport properties in ultrathin silicon nanowires with a diameter of 1–4 nm have been characterized using atomistic simulations and the phonon Boltzmann transport equation. The phonon density of states (PDOS) for ultrathin nanowires approaches a constant value in the vicinity of the Γ point and increases with decreasing diameter, which indicates the increasing importance of the low-frequency phonons as heat carriers. The anharmonic phonon scattering becomes dramatically enhanced with decreasing thickness of the nanowires. In the thinnest nanowire, the scattering rates for phonons above 1 THz are one order of magnitude higher than those in the bulk Si. Below 1 THz, the increase in scattering rates is even much more appreciable. Our numerical calculations revealed that the scattering rates for transverse (longitudinal) acoustic modes follow $\sqrt{\omega}$ ($1/\sqrt{\omega}$) dependence at the low-frequency limit, whereas those for the degenerate flexural modes asymptotically approach a constant value. In addition, the group velocities of phonons are reduced compared with bulk Si except for low-frequency phonons (<1–2 THz depending on the thickness of the nanowires). The increased scattering rates combined with reduced group velocities lead to a severely reduced thermal conductivity contribution from the high-frequency phonons. Although the thermal conductivity contributed by those phonons with low frequencies is instead increased mainly due to the increased PDOS, the total thermal conductivity is still reduced compared to that of the bulk. This work reveals an unexplored mechanism to understand the measured ultralow thermal conductivity of silicon nanowires.

DOI: 10.1103/PhysRevB.97.075441

I. INTRODUCTION

Silicon nanowires (SiNWs) have attracted tremendous interest not only due to their unique structural, electronic, and thermoelectric properties but also from a fundamental physics point of view. The thermal conductivity of SiNWs is of particular importance in terms of affecting their performance and reliability in nanoelectronic devices or finding potential applications in thermoelectrics. Thermal transport in SiNWs has been the subject of several experimental and theoretical studies [1–3]. Experimentally, the thermal conductivity of individual SiNWs with thicknesses ranging from 22 to 115 and 15 to 50 nm has been measured [4,5] and found to be very sensitive to a change in the diameter. A 100-fold decrease in the thermal conductivity of NWs was reported [6,7] when the size was reduced to about ∼50 nm. More recently, SiNWs with diameters of 10–20 nm have been fabricated [8]. The measured thermal conductivity values at room temperature have been found to be ∼1.0 W/mK for smooth and ∼0.1 W/mK for rough-surfaced NWs. This significant reduction in thermal conductivity remarkably improves the energy conversion efficiency, or figure of merit, of thermoelectric devices based on SiNWs [6,7].

Theoretically, thermal transport in low-dimensional systems [one-dimensional (1D) model systems, quasi-1D systems like SiNWs, carbon nanotubes, and two-dimensional (2D) systems] has been the subject of great debate, and in the literature, diverse and even contradictory results can be found. Studies based on numerical simulations and molecular dynamics (MD) methods have indicated [9–18] that the thermal conductivity in low-dimensional systems diverges with the size of the system. Other results based on MD simulations and first-principles methods have shown [19–24] that the thermal conductivity remains finite with the system size of low-dimensional systems.

In the case of thin, pristine SiNWs, nonequilibrium molecular dynamic (NEMD) simulations [21] have shown that the thermal conductivity decreases with the thickness of nanowires down to a critical diameter (1.5–3.5 nm). A further decrease in the thickness results in an increase in thermal conductivity. This nonmonotonic behavior was attributed to the increased frequency of the excited longest-wavelength phonons in the spectra due to confinement effects. Other researchers have obtained similar results for ultrathin nanowires using equilibrium molecular dynamics (EMD) simulations [24–26]. Recent studies [24] have also shown that the thermal conductivity

*wu.li.phys2011@gmail.com

in ultrathin pristine nanowires can attain a value as high as 13 times that for the bulk.

Interestingly, based on NEMD simulations, it has also been reported [15,16] that the thermal transport in extremely thin nanowires (thickness <2.2 nm) does not obey Fourier's law of heat conduction even when the length of the nanowire is much longer than the phonon mean free path. The thermal conductivity diverges due to confinement effects. Recently, the length and diameter dependence of thermal conductivity was revisited [23] for SiNWs with a thickness of 1–14 nm and a length up to 1.2 μm by employing the approach-to-equilibrium molecular dynamics method [27], where no deviation from the Fourier regime was observed.

The effect of confinement or dimensionality reduction on phonon group velocity has also been investigated [28] using the real-space Kubo method [29]. It was found that the confinement effects lead to a substantial reduction in the phonon group velocity in SiNWs compared to that in bulk Si except at extremely low frequencies. The significant difference in the group velocity indicates that the phonon dispersion in SiNWs is essentially different from that of the bulk. The anharmonic phonon-phonon scattering in SiNWs, therefore, is also expected to be very different from that in the bulk. Although the thermal conductivity of thin SiNWs has been extensively studied, the effect of confinement or dimensionality reduction on the anharmonic phonon scattering has not been investigated in detail so far.

In this work, we quantify the confinement effect on the anharmonic phonon scattering rates in ultrathin SiNWs in order to elucidate their role in thermal transport properties of these systems. The phonon dispersion and anharmonic scattering rates are determined by the harmonic and anharmonic interatomic force constants (IFCs), which are calculated using the Stillinger-Weber (SW) interatomic potential [30]. The thermal conductivity is calculated using linearized phonon Boltzmann transport equation (BTE) [31] within the relaxation-time approximation (RTA). It is shown that the anharmonic phonon scattering rates in ultrathin SiNWs become much larger than in the bulk and thus play an import role in reducing the thermal conductivity. The scattering rates increase with decreasing thickness of the NWs and, at low frequencies, exhibit strong branch dependence behavior. The power-law dependences of the scattering rates at the low-frequency limit are also characterized. These results will help us to better understand the phenomenon of thermal transport in one-dimensional materials.

II. METHODOLOGY

In the formalism of the linearized phonon Boltzmann transport equation the thermal conductivity κ of SiNWs is calculated as [31]

$$\kappa = \frac{\hbar^2}{k_B T^2 N V} \sum_{\lambda} \omega_{\lambda}^2 f_{\lambda}^0 \left(1 + f_{\lambda}^0\right) \upsilon_{\lambda} F_{\lambda}, \tag{1}$$

where λ denotes a phonon mode with branch p and wave vector $\mathbf{q}$. k_B is the Boltzmann constant, $\hbar$ is the reduced Plank's constant, T is absolute temperature, V is the volume of the unit cell, and N is the total number of q points uniformly spaced in the Brillouin zone. ω_{λ} is the angular frequency, υ_{λ} represents the group velocity along the SiNW direction, and f_{λ}^0 is the Bose-Einstein distribution function for the phonon population. F_{λ} can be regarded as the phonon mean free path. In the relaxation-time approximation, F_{λ} is calculated as [31]

$$F_{\lambda} = \tau_{\lambda}^0 \upsilon_{\lambda}, \tag{2}$$

where τ_{λ}^0 represents the relaxation time of the phonon mode λ. The inverse of τ_{λ}^0 in RTA is equal to the total scattering rate, which is the sum of the isotope scattering rate and the anharmonic scattering rate. The anharmonic scattering rate can be obtained as the sum of three-phonon transition probabilities, which can be expressed as

$$\Gamma^{+}_{\lambda\lambda'\lambda''} = \frac{\pi\hbar}{4N} \frac{f^0_{\lambda'} - f^0_{\lambda''}}{\omega_{\lambda}\omega_{\lambda'}\omega_{\lambda''}} |V^{+}_{\lambda\lambda'\lambda''}|^2 \delta(\omega_{\lambda} + \omega_{\lambda'} - \omega_{\lambda''}),$$

$$\Gamma^{-}_{\lambda\lambda'\lambda''} = \frac{\pi\hbar}{8N} \frac{f^0_{\lambda'} + f^0_{\lambda''} + 1}{\omega_{\lambda}\omega_{\lambda'}\omega_{\lambda''}} |V^{-}_{\lambda\lambda'\lambda''}|^2 \delta(\omega_{\lambda} - \omega_{\lambda'} - \omega_{\lambda''}), \tag{3}$$

where the plus and minus signs represent absorption and emission processes, respectively, and $V_{\lambda\lambda'\lambda''}$ denotes elements of the scattering matrix which are calculated from anharmonic IFCs [31].

The harmonic and anharmonic IFCs were calculated within a real-space supercell approach using the PHONOPY package [32] for harmonic IFCs and the SHENGBTE [31] package for anharmonic IFCs. A $1 \times 1 \times 2$ supercell size was used in these calculations, and a cutoff value of 5 Å for the interaction range was used to obtain anharmonic IFCs. In all calculations a (001) orientation of SiNWs was considered. SiNWs were constructed by cutting a cylinder of diameter D with length equal to the lattice parameter of bulk Si (5.43 Å at 300 K) from a block of Si with a diamond-lattice atomic structure. Subsequently, the LAMMPS package [33] was employed to relax the structure using a vacuum space equal to 30 Å perpendicular to the axis of the NW in order to avoid any interaction between the periodically repeated images. The interaction between Si atoms was modeled using the SW potential [30]. It is necessary to point out here that empirical potentials such as the SW [30] and Tersoff [34] interatomic potentials provide only a qualitatively acceptable description of the phonon properties of silicon [35–37], although these potentials have successfully been employed to study the structural, energetic, and mechanical properties of Si-based materials [3,38–41]. The translational and rotational invariance of harmonic IFCs was enforced using the *by-construction method* [42]. The translational invariance of anharmonic IFCs was enforced using the Lagrange multiplier technique [31,43]. The SHENGBTE package [31,44] was used to solve the BTE.

III. RESULTS AND DISCUSSION

Phonon dispersion plays a fundamental role in determining anharmonic phonon scattering rates. Figure 1(a) shows the calculated phonon dispersion relations for SiNWs with diameters ranging from 1 to 4 nm and bulk Si for comparison. The immediate consequences of confinement are that there are four acoustic phonon branches in SiNWs compared to three acoustic branches in bulk Si, and two of them are flexural modes with quadratic dispersion. In SiNWs these four branches

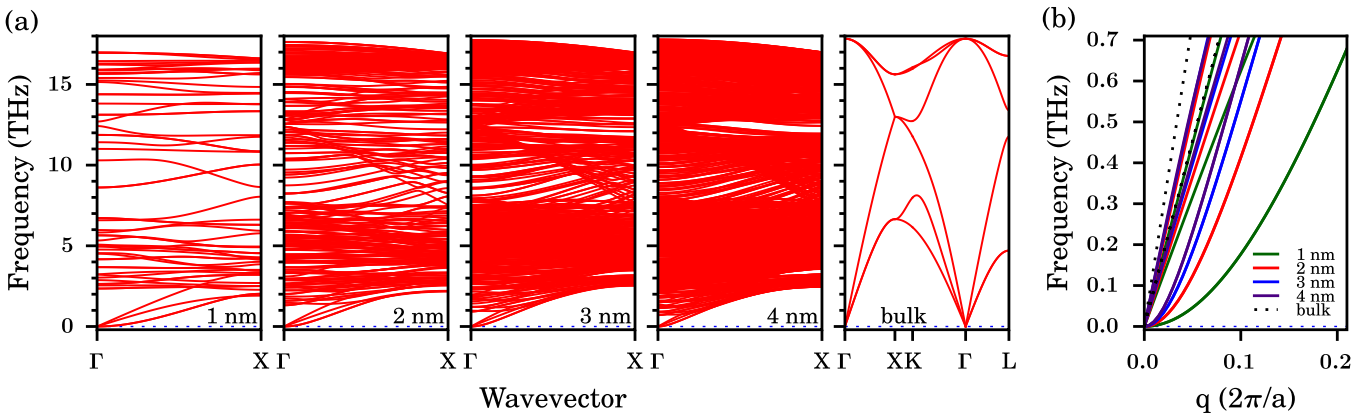

FIG. 1. (a) Phonon dispersions of SiNWs and bulk Si. (b) Comparison of the dispersion relations of acoustic phonons for SiNWs and bulk Si. The lowest acoustic branches with $\omega \propto q^2$ are doubly degenerate for nanowires.

correspond to one rotational and three translational degrees of freedom. All the acoustic phonon modes are softened in SiNWs compared to that in the bulk, and the acoustic phonon frequencies decrease with decreasing thickness of the NWs. The dispersion of flexural modes remains quadratic for larger $\mathbf{q}$ in thinner nanowires. The other two acoustic modes have linear dispersion and correspond to torsional (TA) and longitudinal (LA) vibrational modes.

The phonon density of states (PDOS), normalized by the number of atoms in the unit cell, is shown in Fig. 2 for NWs and bulk Si. The PDOS for NWs is dramatically different from that of bulk Si and also exhibits oscillations. Apparently, the difference becomes more and more appreciable as the diameters of SiNWs decrease, manifesting itself as a more evident confinement effect. The largest difference is found for phonons with a frequency between 2 and 5 THz, which is significantly enhanced compared with that in bulk Si. At the low-frequency limit, the PDOS in bulk Si follows the ω^2 dependence due to the linear dispersion of acoustic phonons and its three-dimensional nature. In contrast, in the 1D SiNWs the linear branches contribute a constant PDOS, and the quadratic branches contribute a divergent $(1/\sqrt{\omega})$ PDOS, which is almost invisible in Fig. 2. The PDOS at low frequency increases with decreasing thickness of the NWs due to softened phonons and reduced volume of the unit cell. The softening of phonons in SiNWs can also be inferred from group velocities, which will be shown in the following discussion.

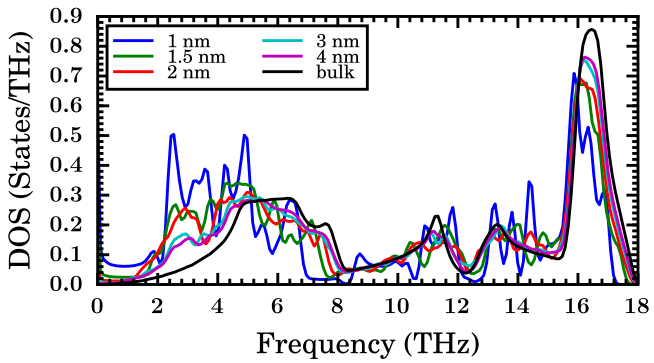

FIG. 2. Phonon density of states for SiNWs and bulk Si.

As the diameters of SiNWs gradually increase, the PDOS will eventually converge to that of bulk Si. As can be seen from Fig. 2, the PDOS at high frequencies (i.e., >8 THz) for 3- and 4-nm-thick NWs becomes quite similar to that of bulk. As revealed previously in Ref. [28], the PDOS in a 10-nm-thick Si NW is almost the same as in the bulk, except the surface phonon modes present between 2 and 3 THz. Typical surface-phonon modes are shown in Fig. 3, where the magnitude of atomic displacements is represented by arrows. As expected, only the surface atoms are involved in these modes, and the contribution of inner atoms (without arrows) is insignificant. Such modes due to surface atoms always appear regardless of the diameter of the SiNW.

The mode-averaged group velocity is calculated in the transport direction using the relation described in Ref. [28]:

$$\upsilon_{\parallel} = \left(\frac{\sum_{\lambda} \upsilon_{\lambda}^2 \delta(\omega - \omega_{\lambda})}{\sum_{\lambda} \delta(\omega - \omega_{\lambda})} \right)^{\frac{1}{2}}. \tag{4}$$

The results are presented in Fig. 4. For frequencies greater than 2 THz, $\upsilon_{\parallel}$ for NWs is significantly reduced compared to that of the bulk, although strong oscillations occur in the 1-nm case, which directly demonstrates the softening of phonons. This is in good agreement with the changes in the PDOS of SiNWs.

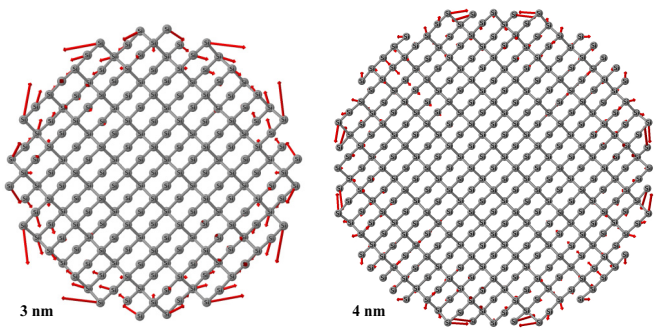

FIG. 3. Typical optical surface-phonon modes present between 2 and 3 THz in SiNW as visualized by JMOL [45]. The magnitude (direction) of displacement of atoms is indicated by red arrows. For better visualization, the length of the arrows is increased by five times the original values.

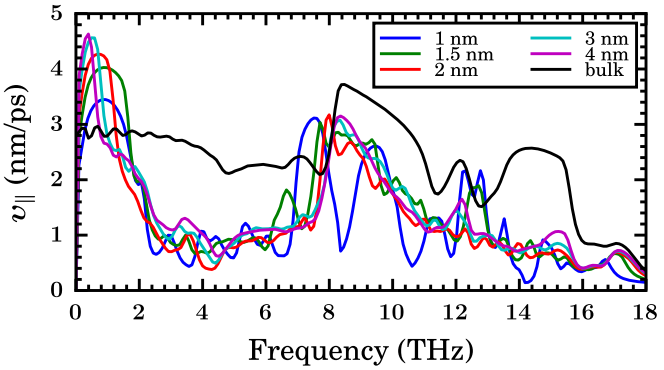

FIG. 4. Mode-averaged group velocity for SiNWs and bulk Si.

Using the real-space Kubo method, reduced group velocities were found earlier for thicker NWs with a diameter ranging from 10 to 55 nm [28], and this effect is likely to persist in SiNWs hundreds of nanometers thick. Most interestingly, $v_{\parallel}$ for low-frequency phonons (<2 THz) in SiNWs first display a quick increase with decreasing frequency, which is mainly due to the absence of optical phonons. Since the threshold for optical phonons decreases with increasing diameter, the quick increase in $v_{\parallel}$ starts to occur at higher frequency in thinner NWs. The quadratic acoustic branches are responsible for the divergent PDOS and vanishing group velocities at the low-frequency limit; therefore, $v_{\parallel}$ further decreases to zero at the low-frequency limit. Due to the fact that acoustic phonons are more softened in thinner NWs, $v_{\parallel}$ decreases with decreasing thickness at low frequencies. It is worth noting that $v_{\parallel}$ in NWs below ∼2 THz is higher than that of the bulk, although the group velocity of the acoustic branches in NWs is smaller than those for the bulk along the particular (Γ-X) direction shown in Fig. 4. Actually, the average taken over modes for bulk along one direction leads to a reduction, which corresponds to a factor of $\sqrt{3}$ in the case of a single and isotropic phonon branch.

Next, we calculate the scattering rates within the RTA approximation for both NWs and bulk Si. As shown in Fig. 5(a), the scattering rates increase with decreasing thickness of the NWs in the whole frequency range. Above 1-THz frequency, the scattering rates for 4-nm-thick NWs are larger than those for the bulk by about 3 times. The scattering rates increase gradually by a few times when the thickness of the NW is reduced from 4 to 1 nm. At low frequencies, the confinement effect on anharmonic scatterings is much more striking than at high frequencies. Below 1 THz, the scattering rates for 4-nm-thick NWs are more than one order of magnitude larger than those for the bulk. More interestingly, the scattering rates at low frequencies show strong branch dependence in NWs, especially in thinner NWs. The scattering rates approach a constant value for the two degenerate flexural branches, whereas those for the TA and LA branches follow $\sqrt{\omega}$ and $1/\sqrt{\omega}$ dependences, respectively. It is interesting to note that for 2D systems like graphene, it is the TA and the LA modes which show constant scattering rates in the low-frequency limits [22,46]. For thicker NWs, the scattering rates start to follow these dependences at lower frequencies. For instance, the two flexural branches have constant scattering rates of 0.005 THz up to ∼0.6-THz frequency in the thinnest NW, while

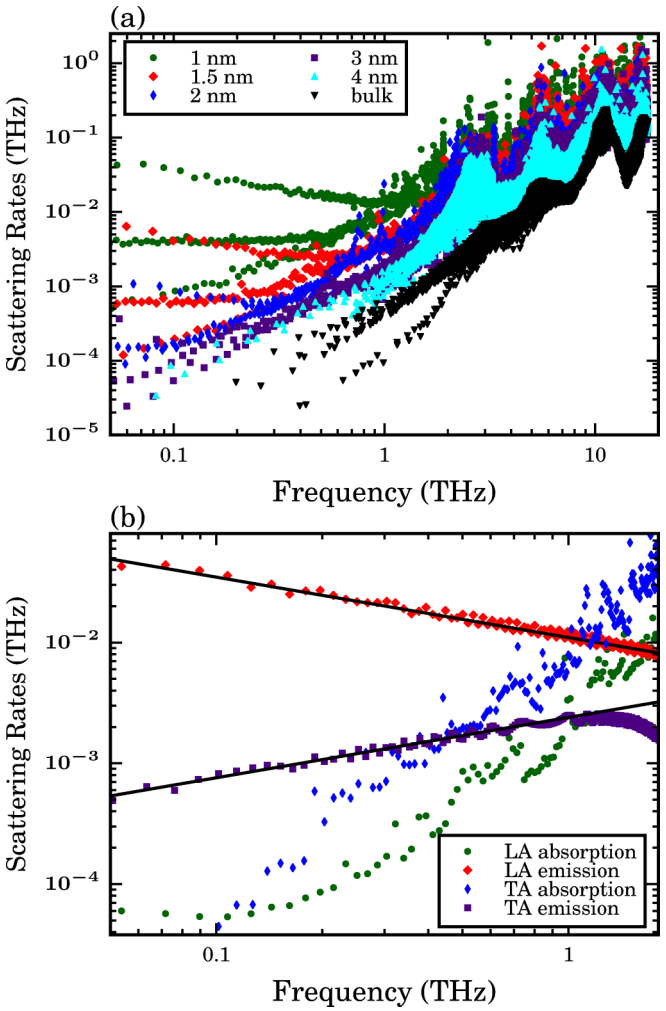

FIG. 5. (a) Anharmonic scattering rates for SiNWs and bulk Si. (b) Contributions to the scattering rates for TA and LA modes due to emission (decay) and absorption processes for 1-nm-thick SiNW. The solid black lines show the fitting of TA (LA) emission to $\sqrt{\omega}$ ($1/\sqrt{\omega}$).

the constant scattering rates remain up to ∼0.1 THz in 2-nm-thick NWs. In the thicker NWs these power-law dependences do not occur down to 0.05 THz. The scattering rates also increase by more than one order of magnitude when the diameter changes from 2 to 1 nm. Some experimental results [8] based on laser-power-dependent Raman spectroscopy have suggested that the anharmonic scattering in 10–20-nm-thick SiNWs remains unchanged compared to that in the bulk. This might be due to approximations used to calculate the temperature dependence of the Stokes/anti-Stokes and Raman shifts in SiNWs. Our results clearly show that the confinement effect drastically changes the scattering rates in NWs, which become much higher than in the bulk, especially at low frequencies.

The anharmonic scattering is enabled only when the momentum and energy conservation conditions are both satisfied. For the flexural modes at low frequencies, only absorption processes are allowed. However, for TA and LA modes at low frequencies, it is the emission process of these modes that dominates the power-law dependences, while the contribution of the absorption processes is negligible, as shown in Fig. 5(b).

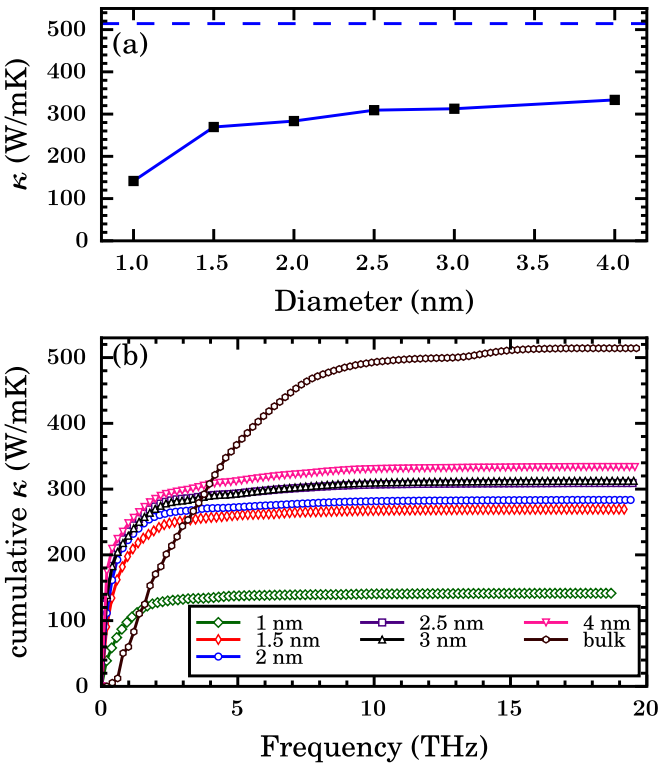

FIG. 6. (a) Thermal conductivity of SiNWs calculated within RTA as a function of diameter. The dashed line represents the thermal conductivity of bulk Si. (b) The cumulative thermal conductivity of SiNWs and bulk Si as a function of frequency.

The room temperature (300 K) thermal conductivity κ calculated based on RTA is shown in Fig. 6(a) for NWs and bulk for comparison. The calculated κ value for bulk Si is 514 W/mK, much higher than the experimental value of ~150 W/mK, reflecting the qualitative but not quantitative nature of the SW potential. The thermal conductivity κ for NWs increases monotonically with diameter, and the increase is very smooth above 1.5 nm. The thermal conductivity κ of a 4-nm-thick NW is 330 W/mK. In order to understand the reduction of κ in NWs, we can look into the cumulative thermal conductivity as a function of phonon frequency, reflecting the contribution of phonons with different energies to the total thermal conductivity. Figure 6(b) shows the cumulative thermal conductivity versus phonons frequency for nanowires and the bulk. In the case of the bulk, phonons above ~2 THz contribute two thirds, i.e., 350 W/mK, to the total thermal conductivity. However, due to increased scattering rates and reduced velocity, especially between 2 and 7 THz, the contribution from these phonons is significantly reduced in the nanowires, and it almost vanishes in the 1-nm case. The low-frequency phonons have an increased contribution to the thermal conductivity, mainly due to the increased phonon density of states. As the thickness decreases, the increase in scattering rates is more striking than the increase in the PDOS. As a result, the low-frequency contribution is smaller in thinner nanowires. The TA modes dominate the contribution at low frequencies.

The ultralow values measured experimentally for NWs are mainly due to the surface roughness scattering, which, however, does not occur in pristine NWs. As mentioned before,

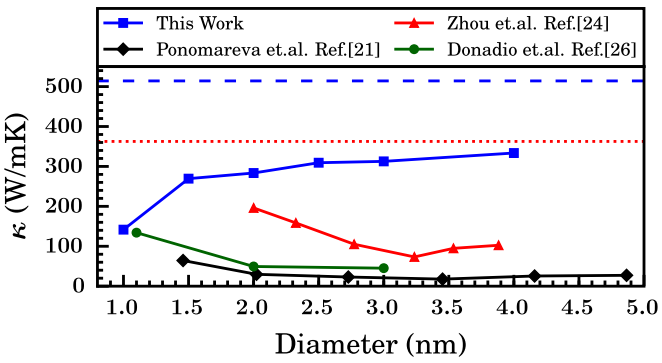

FIG. 7. Thermal conductivity of SiNWs as a function of diameter as reported by Ponomareva *et al.* [21] (diamonds) based on NEMD (SW potential at a temperature of 100 K), Zhou *et al.* [24] (triangles) based on EMD (SW potential at 300 K), and Donadio and Galli [26] (circles) based on EMD (Tersoff potential at 300 K) and from the present work (squares) calculated using BTE within RTA at 300 K. The dotted line represents the thermal conductivity of bulk Si using EMD (SW potential) from Ref. [24], and the dashed line is from the present work.

the increased anharmonic scattering also plays an important role in the reduction of thermal conductivity in NWs. The significant reduction of the group velocity persists in NWs with a thickness of tens of nanometers, suggesting the scattering rates in these NWs should be quite different than in the bulk. Considering the scattering rates decrease very slowly with increasing thickness above 3 nm, we speculate that the scattering rates for NWs tens of nanometers thick are very likely still much higher than those for the bulk, which deserves further clarification.

As shown in Fig. 7, earlier studies based on NEMD [21] and EMD [24–26] simulations have shown that κ of ultrathin NWs exhibits a nonmonotonic behavior. Down to a critical diameter (1.5–3.5 nm depending upon the employed simulation method and force field), κ decreases with the decreasing thickness of NWs. Below this critical thickness κ starts to increase. It was argued [24] that this is because some scattering channels, for example, acoustic + acoustic ↔ optical, are closed due to a shift of the optical phonon modes towards higher frequencies in thinner nanowires. However, in the present work, as can be seen in Fig. 5(a), the scattering rates increase monotonically with decreasing thickness of the NWs, although the optical branches shift towards higher frequencies when the diameter is reduced from 4 to 1 nm. As a result, κ displays a monotonic decrease with decreasing diameter. The thermal conductivity κ is calculated based on RTA, which works very well for bulk Si but might lead to underestimation in nanowires. We tried to solve the phonon mean free path F_λ from the iterative scheme [31]; however, we were not able to get a converged solution. This might suggest the thermal conductivity in one-dimensional system diverges, which has been debated for a long time [13–16,23,24]. This could also possibly be due to some not-yet-identified numerical noise. We note that Ref. [24] obtained a converged κ from iterative BTE. Nevertheless, whether or not κ in a one-dimensional system diverges and κ in NWs possesses nonmonotonic diameter dependence deserves further study. At least at the RTA level, κ does not diverge and increases monotonically with diameter.

The thermal conductivity κ for NWs and bulk Si calculated with BTE are quite high compared to the values reported earlier in the literature [21,24–26] using MD simulations, as shown in Fig. 7. He *et al.* [37] compared in detail the BTE and MD methods for bulk systems. First, the phonon distribution is treated classically within MD simulations, while BTE involves Bose-Einstein statistics. The classical statistics in MD leads to underestimated κ below the Debye temperature. More importantly, extremely large samples should be used in MD simulations to ensure convergence. However, in the literature convergence tests have often been limited to relatively modest sizes (several thousand atoms) due to high computational costs [37]. This also explains the difference in the κ values calculated for the same material with the same MD method but with different simulation parameters. In the case of bulk Si, systems as large as several hundred thousand atoms are required, using either EMD or NEMD [37]. Considering lower-frequency phonons with longer mean free paths dominate thermal transport, it becomes more difficult to achieve convergence in pristine NWs than in the bulk. From the BTE side, RTA typically underestimates κ, indicating that the actual difference between BTE and MD is even larger than shown in Fig. 7. Nevertheless, a full understanding of the discrepancy in the results of the BTE and MD methods remains an open problem.

IV. CONCLUSION

In summary, using atomistic simulations and the phonon Boltzmann transport equation, we have investigated the lattice dynamics and phonon transport properties of ultrathin SiNWs, e.g., phonon dispersion, the density of states, group velocities, phonon scattering rates, and thermal conductivities. Our results clearly illustrate the effect of confinement on the phonon transport ability of SiNWs. Specifically, the confinement in SiNWs leads to greatly softened phonon dispersion; thus, the phonon group velocities are severely reduced for frequencies greater than 2 THz. In addition, the anharmonic scattering rates are intensively enhanced in SiNWs, which in turn plays a significant role in reducing the thermal conductivity. For frequencies greater than 1 THz, the scattering rates in SiNWs are many times larger than in the bulk. At low frequency the difference is even much larger. The slow decrease in the scattering rates with the diameter, especially for thicker NWs, indicates that the scattering rates in NWs tens of nanometers thick should remain much larger than in the bulk. For thinner NWs, the scattering rates exhibit a clear power-law dependence below 1 THz, and this dependence is gradually shifted towards lower frequency with increasing thickness. The phonon group velocity in NWs is also reduced compared to bulk Si, except at low frequencies below 1–2 THz, depending upon the thickness. The increased scattering rates combined with reduced group velocity lead to reduced thermal conductivity in pristine nanowires. Our findings highlight the distinctions in the lattice dynamics and phonon scattering between one-dimensional and bulk systems.

ACKNOWLEDGMENTS

We thank Dr. A. S. Nissimagoudar and Dr. J. Ma (Shenzhen University, China) for helpful discussions and suggestions. Z.R. and W.L. acknowledge support from the National Natural Science Foundation of China under Grant No. 11704258 and the Natural Science Foundation of Guangdong Province under Grant No. 2017A030310377. L.Z. acknowledges the financial support from the National Natural Science Foundation of China (Grants No. 11504122 and No. 11704141) and the Natural Science Foundation of the Higher Education Institutions of Jiangsu Province (Grant No. 15KJB140001).

[1] S. G. Volz and G. Chen, Appl. Phys. Lett. **75**, 2056 (1999).
[2] S. Volz, D. Lemonnier, and J.-B. Saulnier, Microscale Thermophys. Eng. **5**, 191 (2001).
[3] S.-C. Wang, X.-G. Liang, X.-H. Xu, and T. Ohara, J. Appl. Phys. **105**, 014316 (2009).
[4] D. Li, Y. Wu, P. Kim, L. Shi, P. Yang, and A. Majumdar, Appl. Phys. Lett. **83**, 2934 (2003).
[5] R. Chen, A. I. Hochbaum, P. Murphy, J. Moore, P. Yang, and A. Majumdar, Phys. Rev. Lett. **101**, 105501 (2008).
[6] A. I. Boukai, Y. Bunimovich, J. Tahir-Kheli, J.-K. Yu, W. A. Goddard Iii, and J. R. Heath, Nature (London) **451**, 168 (2008).
[7] A. I. Hochbaum, R. Chen, R. D. Delgado, W. Liang, E. C. Garnett, M. Najarian, A. Majumdar, and P. Yang, Nature (London) **451**, 163 (2008).
[8] D. Fan, H. Sigg, R. Spolenak, and Y. Ekinci, Phys. Rev. B **96**, 115307 (2017).
[9] P. G. Klemens and D. F. Pedraza, Carbon **32**, 735 (1994).
[10] S. Lepri, R. Livi, and A. Politi, Phys. Rep. **377**, 1 (2003).
[11] J.-S. Wang and B. Li, Phys. Rev. Lett. **92**, 074302 (2004).
[12] S. Lepri, R. Livi, and A. Politi, Chaos **15**, 015118 (2005).
[13] G. Zhang and B. Li, J. Chem. Phys. **123**, 014705 (2005).
[14] C. W. Chang, D. Okawa, H. Garcia, A. Majumdar, and A. Zettl, Phys. Rev. Lett. **101**, 075903 (2008).
[15] Y. Xueming, C. T. Albert, and T. Rong, Nanotechnology **21**, 155704 (2010).
[16] N. Yang, G. Zhang, and B. Li, Nano Today **5**, 85 (2010).
[17] L. Nicolin and D. Segal, Phys. Rev. E **81**, 040102 (2010).
[18] L. Wang, B. Hu, and B. Li, Phys. Rev. E **88**, 052112 (2013).
[19] N. Mingo and D. A. Broido, Nano Lett. **5**, 1221 (2005).
[20] D. Donadio and G. Galli, Phys. Rev. Lett. **99**, 255502 (2007).
[21] I. Ponomareva, D. Srivastava, and M. Menon, Nano Lett. **7**, 1155 (2007).
[22] N. Bonini, J. Garg, and N. Marzari, Nano Lett. **12**, 2673 (2012).
[23] H. Zaoui, P. L. Palla, F. Cleri, and E. Lampin, Phys. Rev. B **95**, 104309 (2017).
[24] Y. Zhou, X. Zhang, and M. Hu, Nano Lett. **17**, 1269 (2017).
[25] D. Donadio and G. Galli, Phys. Rev. Lett. **102**, 195901 (2009).
[26] D. Donadio and G. Galli, Nano Lett. **10**, 847 (2010).
[27] E. Lampin, P. L. Palla, P. A. Francioso, and F. Cleri, J. Appl. Phys. **114**, 033525 (2013).
[28] L. Zhu, B. Li, and W. Li, Phys. Rev. B **94**, 115420 (2016).

[29] W. Li, H. Sevinçli, S. Roche, and G. Cuniberti, Phys. Rev. B **83**, 155416 (2011).
[30] F. H. Stillinger and T. A. Weber, Phys. Rev. B **31**, 5262 (1985).
[31] W. Li, J. Carrete, N. A. Katcho, and N. Mingo, Comput. Phys. Commun. **185**, 1747 (2014).
[32] A. Togo and I. Tanaka, Scripta Mater. **108**, 1 (2015).
[33] S. Plimpton, J. Comput. Phys. **117**, 1 (1995).
[34] J. Tersoff, Phys. Rev. B **37**, 6991 (1988).
[35] E. R. Cowley, Phys. Rev. Lett. **60**, 2379 (1988).
[36] D. A. Broido, A. Ward, and N. Mingo, Phys. Rev. B **72**, 014308 (2005).
[37] Y. He, I. Savic, D. Donadio, and G. Galli, Phys. Chem. Chem. Phys. **14**, 16209 (2012).
[38] X. P. Li, G. Chen, P. B. Allen, and J. Q. Broughton, Phys. Rev. B **38**, 3331 (1988).
[39] M. Karimi, H. Yates, J. R. Ray, T. Kaplan, and M. Mostoller, Phys. Rev. B **58**, 6019 (1998).
[40] M. Menon, D. Srivastava, I. Ponomareva, and L. A. Chernozatonskii, Phys. Rev. B **70**, 125313 (2004).
[41] I. Ponomareva, M. Menon, D. Srivastava, and A. N. Andriotis, Phys. Rev. Lett. **95**, 265502 (2005).
[42] J. Carrete, W. Li, L. Lindsay, D. A. Broido, L. J. Gallego, and N. Mingo, Mater. Res. Lett. **4**, 204 (2016).
[43] W. Li, L. Lindsay, D. A. Broido, D. A. Stewart, and N. Mingo, Phys. Rev. B **86**, 174307 (2012).
[44] W. Li, N. Mingo, L. Lindsay, D. A. Broido, D. A. Stewart, and N. A. Katcho, Phys. Rev. B **85**, 195436 (2012).
[45] JMOL, an open-source JAVA viewer for chemical structures in 3D, http://www.jmol.org/
[46] L. Lindsay, W. Li, J. Carrete, N. Mingo, D. A. Broido, and T. L. Reinecke, Phys. Rev. B **89**, 155426 (2014).